Atmos. Chem. Phys. Discuss., 12, 1979–2024, 2012
www.atmos-chem-phys-discuss.net/12/1979/2012/
doi:10.5194/acpd-12-1979-2012

Atmospheric Chemistry and Physics Discussions

A Tropospheric ozone maximum over the equatorial southern Indian Ocean

L. Zhang[1,2], Q. B. Li[1,2], L. T. Murray[3], M. Luo[4], H. Liu[5], J. H. Jiang[4], Y. Mao[1,2], D. Chen[1,2], M. Gao[1,2], and N. Livesey[4]

[1]Department of Atmospheric and Oceanic Sciences, University of California, Los Angeles, CA, USA
[2]Joint Institute for Regional Earth System Science and Engineering, University of California, Los Angeles, CA, USA
[3]School of Engineering and Applied Sciences, Harvard University, Cambridge, MA, USA
[4]Jet Propulsion Laboratory, California Institute of Technology, CA, USA
[5]National Institute of Aerospace, Hampton, VA, USA

Received: 13 December 2011 – Accepted: 17 January 2012 – Published: 20 January 2012

Correspondence to: Q. B. Li (qli@atmos.ucla.edu)

Published by Copernicus Publications on behalf of the European Geosciences Union.

Abstract

We examine the distribution of tropical tropospheric ozone (O_3) from the Microwave Limb Sounder (MLS) and the Tropospheric Emission Spectrometer (TES) by using a global three-dimensional model of tropospheric chemistry (GEOS-Chem). MLS and TES observations of tropospheric O_3 during 2005 to 2009 reveal a distinct, persistent O_3 maximum, both in mixing ratio and tropospheric column, in May over the Equatorial Southern Indian Ocean (ESIO). The maximum is most pronounced in 2006 and 2008 and less evident in the other three years. This feature is also consistent with the total column O_3 observations from the Ozone Mapping Instrument (OMI) and the Atmospheric Infrared Sounder (AIRS). Model results reproduce the observed May O_3 maximum and the associated interannual variability. The origin of the maximum reflects a complex interplay of chemical and dynamic factors. The O_3 maximum is dominated by the O_3 production driven by lightning nitrogen oxides (NO_x) emissions, which accounts for 62 % of the tropospheric column O_3 in May 2006. We find the contribution from biomass burning, soil, anthropogenic and biogenic sources to the O_3 maximum are rather small. The O_3 productions in the lightning outflow from Central Africa and South America both peak in May and are directly responsible for the O_3 maximum over the western ESIO. The lightning outflow from Equatorial Asia dominates over the eastern ESIO. The interannual variability of the O_3 maximum is driven largely by the anomalous anti-cyclones over the southern Indian Ocean in May of 2006 and 2008. The lightning outflow from Central Africa and South America is effectively entrained by the anti-cyclones followed by northward transport to the ESIO.

1 Introduction

Ozone (O_3) in the tropical upper troposphere is an effective greenhouse gas (Lacis et al., 1990). Ozone is also an important tropospheric oxidant and modulates the oxidizing power of the troposphere through photolysis in the presence of water vapor

ACPD
12, 1979–2024, 2012

that generates hydroxyl radical (OH), the main atmospheric oxidant (Levy, 1971; Logan et al., 1981). Production of tropical tropospheric O_3 is driven by nitrogen oxides (NO_x = NO + NO_2) emitted from primarily lightning (e.g., Sauvage et al., 2007; Ziemke et al., 2009) and biomass burning (e.g., Fishman et al., 1990; Jacob et al., 1996; Thompson et al., 2001; Logan et al., 2008). Large-scale dynamics is another prominent factor in controlling tropical tropospheric O_3 distributions (e.g., Chandra et al., 2009; Zhang et al., 2011; Oman et al., 2011, and references therein).

The present study is motivated by an observed tropospheric O_3 maximum in May over the southern tropical Indian Ocean from observations by the Microwave Limb Sounder (MLS), the Tropospheric Emission Spectrometer (TES), the Ozone Mapping Instrument (OMI) aboard the Aura satellite, and the Atmospheric Infrared Sounder (AIRS) aboard Aqua (detailed discussions in Sect. 4). Such an O_3 maximum was indicated in previous observations (e.g., Komala, 1996; Ziemke et al., 2009). We investigate here the origin of this O_3 maximum and its interannual variability by interpreting the satellite observations using a global three-dimensional (3-D) chemical transport model (CTM). We intend to delineate the relative influence of biomass burning, lightning, and dynamics in controlling the O_3 maximum. Much of our analysis focuses on the Equatorial Southern Indian Ocean (10° S–equator (EQ) latitudes, 60° E–125° E longitudes), referred to hereafter as ESIO (the shaded rectangle in Fig. 1).

We give a brief description of the observations in Sect. 2. Section 3 describes the GEOS-Chem model and simulations. Seasonal variations of tropospheric O_3 in 2006 over the ESIO are discussed in Sect. 4. The lightning impact on tropospheric O_3 over the region is examined in Sect. 5. Section 6 investigates the interannual variability of the tropospheric O_3 enhancements over the ESIO. The results and discussion are summarized in Sect. 7.

ACPD
12, 1979–2024, 2012

2 Observations

2.1 MLS O_3

The Microwave Limb Sounder (MLS) (Waters et al., 2006) aboard the EOS Aura spacecraft (Schoeberl et al., 2006) has been measuring atmospheric parameters since August 2004. MLS uses microwave limb sounding to measure temperature and chemical constituents, including CO, O_3, water vapor, and cloud ice water content in the upper troposphere and the lower stratosphere. MLS measurements in the upper troposphere are generally not degraded by the presence of clouds and aerosols because the typical cloud and aerosol particle sizes are generally much smaller than the measurement wavelengths. MLS measures ~3500 vertical profiles per day along a sun-synchronous polar orbit, with an equator-crossing time of ~13:45 local time. The data are produced on pressure surfaces from 316 to 0.1 hPa. MLS data has a vertical resolution of ~3–4 km and horizontal resolutions of ~7 km across-track and ~200–300 km along-track (Livesey et al., 2006). We use here O_3 from MLS Version 3.3 (v3.3) Level 2 data (Livesey et al., 2011). Livesey et al. (2008) reported the validation of an earlier version of MLS O_3 (v2.2). The estimated accuracies of MLS v2.2 O_3 are ~20 ppbv (+20 %) at 215 hPa and 40 ppbv (+5 %) at 147 hPa. The systematic errors of MLS v3.3 O_3 are consistent with those of v2.2 (Livesey et al., 2011). Our analysis focuses on the observations at 147 and 215 hPa in the upper troposphere. For the present study, the observations are averaged onto 2° latitude × 5° longitude grids for every five days from 2005 to 2009.

2.2 TES O_3

The Tropospheric Emission Spectrometer (TES) is an infrared, high-resolution, Fourier Transform spectrometer covering the spectral range between 3.3 and 15.4 µm (Beer et al., 2001, 2006). It was launched on board Aura (Schoeberl et al., 2006) in July 2004 in a sun-synchronous polar orbit. TES provides global vertically resolved measurements

ACPD
12, 1979–2024, 2012

A Tropospheric ozone maximum over the Indian Ocean

L. Zhang et al.

of tropospheric O_3, CO and other atmospheric constituents. TES retrievals have been previously described by Bowman et al. (2006) and Kulawik et al. (2006). For the O_3 retrieval, the prior information is derived from a global model simulation using the MOZART model (Brasseur et al., 1998). Typical TES averaging kernels for O_3 are shown in Worden et al. (2007) and Shim et al. (2009). We use data from TES global surveys that include 16 orbits per global survey, over a time period of 26 h (Osterman et al., 2008). The nadir O_3 vertical profiles are spaced ∼182 km apart along the orbit track and have a footprint of 5 km by 8 km (Beer et al., 2001). Under clear sky the vertical resolution of TES O_3 profile retrievals is typically 6 km in the tropics (Jourdain et al., 2007). We use here Version 4 (v4) Level 3 of TES O_3, including mixing ratio, TCO, and total column O_3 data from 2005 to 2009. These data are binned onto a grid of 2° (latitude) × 4° (longitude). Validation of TES tropospheric O_3 retrievals against ozonesonde and lidar measurements shows that is a positive bias of ∼3–10 ppbv (Nassar et al., 2008). The bias of TES TCOs is known to be high by ∼4 DU in comparison with ozonesonde data (Osterman et al., 2008).

2.3 OMI and AIRS total column O_3

The Ozone Monitoring Instrument (OMI) aboard Aura is a nadir-viewing, wide-swath hyper-spectral imaging spectrometer that provides daily global coverage with high spatial and spectral resolutions (Levelt et al., 2006a). It detects backscattered solar radiance in the ultraviolet-visible wavelengths (0.27 to 0.5 µm) to measure column O_3 and other trace constituents and aerosols (Levelt et al., 2006b). OMI data has a spatial resolution of 13 × 24 km^2 at nadir. Here we use the OMI-TOMS total column O_3 derived from the TOMS (version 8) algorithm. Validation of the OMI total column O_3 against ground-based observations by Brewer/Dobson spectrophotometer instruments shows generally a better than 1 % agreement (Balis et al., 2007; McPeters et al., 2008).

The Atmospheric Infrared Sounder (AIRS) (Aumann et al., 2003) is a high spectral resolution infrared sounder flown aboard the Aqua spacecraft (Parkinson, 2003) and has been operational since September 2002. Aqua is in a sun-synchronous polar orbit,

ACPD
12, 1979–2024, 2012

with an equatorial crossing of ∼13:30 local time, covering the earth twice a day. Validation of AIRS total column O_3 against ground-based Brewer/Dobson measurements shows a bias of less than 4 % and a root-mean-square error of approximately 8 % (Divakarla et al., 2008). We use AIRS Version 5 (V5) Level 3 total column O_3 binned onto a 1° (latitude) × 1° (longitude) grid from 2005 to 2009.

3 GEOS-Chem model description and simulations

GEOS-Chem is a global 3-D CTM driven by assimilated meteorological observations from the Goddard Earth Observing System (GEOS) of the NASA Global Modeling and Assimilation Office (GMAO) (Bey et al., 2001). We use GEOS-Chem version 8-01-04 (http://acmg.seas.harvard.edu/geos/) driven by GEOS-4 and GEOS-5 meteorological fields with 6-h temporal resolution (3-h for surface variables and mixing depths), 2° (latitude) × 2.5° (longitude) horizontal resolution, and 30 (GEOS-4) or 47 (GEOS-5) vertical layers between the surface and 0.01 hPa. The GEOS-Chem model includes a detailed description of tropospheric O_3-NO_x-hydrocarbon chemistry coupled with aerosol chemistry (Bey et al., 2001). Gas phase chemical reaction rates and photolysis cross sections are taken from Sander et al. (2000). Photolysis frequencies are computed using the Fast-J algorithm (Wild et al., 2000). The cross-tropopause O_3 flux is specified with the Synoz method (McLinden et al., 2000) while the cross-tropopause NO_y flux is calculated from N_2O oxidation in the model stratosphere (Bey et al., 2001). Global net cross-tropopause fluxes of O_3 and NO_y are 495 Tg O_3 yr^{-1} and 0.5 Tg N yr^{-1}, respectively (Hudman et al., 2007).

Tracer advection is computed every 15 min with a flux-form semi-Lagrangian method (Lin and Rood, 1996). Tracer moist convection is computed using the GEOS convective, entrainment, and detrainment mass fluxes as described by Allen et al. (1996a, b). The deep convection scheme of GEOS-4 is based on Zhang and McFarlane (1995), and the shallow convection treatment follows Hack (1994). GEOS-5 convection is parameterized using the relaxed Arakawa-Schubert scheme (Moorthi and Suarez, 1992).

ACPD
12, 1979–2024, 2012

Emissions of lightning NO_x in GEOS-Chem are computed locally in deep convection events following the scheme of Price and Rind (1992) that relates flash rates to convective cloud top heights. The NO_x emissions are vertically distributed following the profile from Pickering et al. (1998) where 55–75 % of the emissions are above 8 km. Implementation of the lightning source in GEOS-Chem is as described by Wang et al. (1998) with some recent updates (Hudman et al., 2007; Sauvage et al., 2007; Nassar et al., 2009; Jourdain et al., 2010; Murray et al., 2012). The model also includes two alternative lightning schemes that link flash rates to either convective precipitation or upward convective mass flux, following Allen and Pickering (2002). The lightning modules as implemented in GEOS-Chem based on the aforementioned three schemes are hereafter referred to as CTH, PREC, and MFLUX, respectively. To improve the spatial distribution of lightning in the model, the spatial distribution of lightning is scaled to reproduce seasonal mean lightning flash rates to match the climatological satellite observations of lightning flashes from the Optical Transient Detector and Lightning Imaging Sensor (OTD/LIS) High Resolution Monthly Climatology (HRMC) v2.2 product (Christian et al., 2003). Globally the lightning NO_x source is scaled to 6 $Tg\,N\,yr^{-1}$ (Martin et al., 2007; Hudman et al., 2007; Sauvage et al., 2007).

Lightning flash rates in global atmospheric models are usually parameterized from functions of proxies of deep convection, enabling the linking of lightning NO_x emissions with the concurrent convective transport of surface precursors. We test here those based on convective cloud top heights (CTH) (Price and Rind, 1992, 1993, 1994), upward convective mass flux (MFLUX) (Allen et al., 2000), and total convective precipitation (PREC) (Allen and Pickering, 2002) using 6-h mean archived meteorology from the Goddard Earth Observing System Data Assimilation System (GEOS DAS) version 5.1.0. Once the flash rate is determined for a grid box, a NO_x per flash yield is applied, and the NO_x emissions are vertically distributed throughout the column following the probability distribution functions of Pickering et al. (1998). The CTH parameterization was originally implemented by Wang et al. (1998) and MFLUX and PREC by Murray et al. (2012). Each parameterization shows little skill in matching the spatial and seasonal distribution of flash rates observed in the long-term mean Lightning Imaging Sensor and Optical Transient Detector (LIS/OTD) High Resolution Monthly Climatology (HRMC) v2.2 satellite product, and therefore techniques have been variously implemented to constrain the flash rates derived from the GEOS met fields (e.g., Sauvage et al., 2007; Jourdain et al., 2010; Allen et al., 2010; Murray et al., 2012). We also use here an optional "local redistribution" as implemented by Murray et al. (2012). Due to the lack of GEOS-5 meteorological fields during the observation period of the HRMC product (May 1995 through December 2005), we determine the constraint using the long-term monthly mean from all available months of GEOS v5.1.0 meteorology (January 2004 through August 2008).

Biomass burning emissions are from GFED v2 that resolves the interannual variability of biomass burning emissions (van der Werf et al., 2006; Randerson et al., 2006). GFED v2 is derived using satellite observations including active fire counts and burned areas in conjunction with the Carnegie-Ames-Stanford-Approach (CASA) biogeochemical model. Carbon emissions are calculated as the product of burned area, fuel load and combustion completeness. Burned area is derived using the active fire and 500-m burned area datasets from the Moderate Resolution Imaging Spectroradiometer (MODIS) as described by Giglio et al. (2006). The original GFED v2 inventory has a spatial resolution of 1° (latitude) × 1° (longitude) and a monthly temporal resolution. The emissions are re-sampled to 2° (latitude) × 2.5° (longitude) grids for use in our GEOS-Chem simulations. Forest fires typically last from several days to weeks as seen in MODIS active fires (Giglio et al., 2003). Therefore, we re-sampled GFED v2 monthly emissions to an 8-day time step according to MODIS 8-day active fire counts (Chen et al., 2009). The GFED v2 8-day emissions are used for the model simulations presented here unless stated otherwise.

The fossil fuel emissions are from the Emission Database for Global Atmospheric Research (EDGAR) inventory for NO_x, CO, and SO_2 (Olivier et al., 2001) and from the Global Emission Inventory Activity (GEIA) for other chemical compounds (Benkovitz et al., 1996) with additional updates as described by Hudman et al. (2007). Asian

ACPD
12, 1979–2024, 2012

A Tropospheric ozone maximum over the Indian Ocean

L. Zhang et al.

anthropogenic emissions are updated with the estimates from Zhang et al. (2009). Biofuel emissions are from Yevich and Logan (2003). The biogenic VOCs emissions are based on the Model of Emissions of Gases and Aerosols from Nature (MEGAN) inventory (Guenther et al., 2006).

We conducted model simulations from 2005 to 2009 driven by either GEOS-4 or GEOS-5 meteorological data. Our analysis focuses on the results for 2006. Justifications for these simulations are provided where appropriate. The details for these simulations are summarized in Table 1. For direct comparison with the satellite observations, we extracted model results at the time and location of the observations and applied the same spatial and temporal averaging as we did for the observations.

4 Seasonal variation of tropospheric O_3 over the ESIO

4.1 MLS upper tropospheric O_3

Figure 2 shows MLS O_3 concentrations at 20° S–20° N, averaged between 60° E and 125° E for 2006. The values are 5-day averages. South of the equator at 215 hPa the O_3 concentrations show a broad maximum during May and early June when the concentrations are higher by 20 to 30 ppbv relative to those during March and April. This maximum is the focus of the present study. There is a secondary peak during late June and early July with maximum concentrations confined to the region between 10° S and 20° S latitudes. Similar yet considerably smaller enhancements are also evident at 147 hPa during May and June. The O_3 enhancements during October and November, seen at both 215 and 147 hPa, are largely because of the extensive fires in Equatorial Asia (mostly in southern Borneo and Sumatra) that lasted from September through November 2006 and the dynamic changes pertained to the 2006 El Niño (Zhang et al., 2011, and references therein). Figure 3 shows time series of MLS O_3 at 215 and 147 hPa averaged over the entire ESIO domain (Fig. 1) for 2006. Again, broad enhancements of O_3 are evident during May–June with maximum O_3 concentrations exceeding 55 ppbv at 215 hPa and 100 ppbv at 147 hPa.

ACPD
12, 1979–2024, 2012

4.2 TES middle and upper tropospheric O_3

TES tropospheric O_3 also shows a distinct maximum in May 2006 over the ESIO, and the enhancement extends throughout the middle and upper troposphere with peak values above 50 ppbv (Fig. 4). The pronounced and broad O_3 enhancements in the middle and upper troposphere during September through December are largely because of the 2006 Indonesian fires in Equatorial Asia (Logan et al., 2008; Nassar et al., 2009; Zhang et al., 2011). Figure 5 shows TES monthly tropospheric O_3 and TCO over the ESIO for 2006. Both tropospheric O_3 and TCO show seasonal maxima in May and during September through November. The largest O_3 enhancements in May are in the middle to upper troposphere, with peak mixing ratios over 50 ppbv at 464 hPa. The peak values of TES TCO are over 30 DU in May and in October and November.

5 Lightning impact on tropospheric O_3 over the ESIO

5.1 Sensitivity to lightning parameterization

GEOS-Chem simulations of tropospheric O_3 undoubtedly bear the differences of the lightning parameterizations and the meteorological data used. To examine this sensitivity, we conducted six sensitivity simulations (summarized in Table 1), driven by GEOS-4 or GEOS-5 meteorological data, using the different lightning parameterizations (see Sect. 3). Model TCO averaged over the ESIO are compared against TES data and shown in Fig. 6. For direct comparison with the observations, we calculated TCO from model results at the time and location of TES observations and applied the same monthly averaging as we did for the observations (Sect. 4). In general, when comparing TES profiles with other measurements, it is essential to take into account the different sensitivities of the instruments by applying TES averaging kernels (Lou et al., 2007; Worden et al., 2007). However, comparing columns rather than individual profiles significantly reduces the error due to averaging over pressure ranges

ACPD
12, 1979–2024, 2012

larger than the TES vertical resolution, 1.5 % for O_3 columns averages as compared to 16.5 % for the average profile error between the surface and 35 km altitude (Osterman et al., 2008). As such, we did not convolute TES averaging kernels with GEOS-Chem simulated O_3 profiles when calculating model TCOs.

Model simulations A1–A4 were driven by GEOS-4 meteorological data. A1 and A2 used the same CTH lightning parameterization, but A2 used the local redistribution of lightning flash rates based on LIS/OTD observations (Sect. 3) while A1 did not. A3 and A4 used the MFLUX and the PREC lightning parameterizations, respectively, and neither included the local redistribution factors. Given the way lightning is linked to deep convection in the model, the different deep convection parameterizations used in GEOS-4 and GEOS-5 will also lead to differences in the lightning NO_x emissions in the model. To examine this sensitivity, we conducted two additional simulations driven by GEOS-5 meteorological data, B1 and B2. Other than the GEOS-5 meteorological data used, B1 and B2 mirror A1 and A2, respectively.

Figure 6 shows that B1, driven by GEOS-5 data and with the CTH lightning parameterization, best captures the seasonal variation of TES TCO, including the enhancement in May 2006. Model results are consistently lower than the observations by up to 4 DU for all months. That is not a systematic bias necessarily because TES TCOs are known to be biased high by ~4 DU in comparison with ozonesonde data (Osterman et al., 2008). A1, driven by GEOS-4 data and with the CTH lightning parameterization, significantly underestimates the TCO throughout the year. A3 and A4, driven by GEOS-4 data and with the MFLUX and the PREC lightning parameterizations, show no apparent relative enhancements of TCO in May 2006. Neither reproduces the observed TCO seasonal variation. A2 and B2, using a local redistribution factor of lightning flash rates based on LIS/OTD data, show no obvious improvements to A1 and B1. In fact, both A2 and B2 show substantially lower TCOs in comparison with not only A1 and B1, respectively, but also TES observations. Therefore, we choose as our standard simulation the GEOS-Chem simulation driven by GEOS-5 meteorological data using the CTH lightning parameterization without local redistribution factor for flash rates.

ACPD
12, 1979–2024, 2012

5.2 Regional lightning NO_x emissions in the tropics

To examine the relative contributions from lightning, we focus our analysis on the following geographical regions (Fig. 1): the tropical Indian Ocean (10° S–10° N, 40° E–95° E), South Asia (10° N–30° N, 70° E–110° E), Equatorial Asia (10° S–10° N, 95° E–150° E), Central Africa (10° S–20° N, 20° W–40° E) and South America (20° S–15° N, 85° W–35° W). Figure 7 shows the seasonal variations of monthly lightning NO_x emissions from the aforementioned five regions. Again, these results are from the standard simulation driven by GEOS-5 meteorological data and with the CTH lightning parameterization (simulation B1). The seasonal variations of lightning NO_x vary considerably among the regions. Lightning NO_x emissions from South Asia show a broad maximum during June–August, the intense phase of the Asian monsoon with abundant convective activities. Central African lightning NO_x emissions are largest first in May and then in September–October. Lightning NO_x emissions from South America show peaks during March through April and then October through December. Equatorial Asia lightning NO_x emissions show little seasonal variation and are at least a factor of two smaller than those from South Asia, Central Africa and South America. Lightning NO_x emissions from the tropical Indian Ocean are smallest among the five regions but peak in May. In May, the largest lightning NO_x emissions are from Central Africa and South America.

5.3 Lightning contribution to tropospheric O_3 over the ESIO

We conducted several sensitivity simulations for 2006 to quantify the relative contributions to the tropical tropospheric O_3 over the ESIO from NO_x emissions from lightning, biomass burning, soil, stratospheric downward flux, anthropogenic activities and biogenic sources by shutting off these sources individually. The difference between these sensitivity simulations and the standard simulation are thus the contributions from the corresponding sources except the stratospheric downward flux. Here the contribution of the stratospheric downward flux is quantified by the tagged O_x simulation. Again,

ACPD
12, 1979–2024, 2012

all simulations are driven by GEOS-5 meteorological data and with the CTH lightning parameterization. The resulting contributions, calculated as monthly TCOs averaged over the ESIO, are shown in Fig. 8.

Lightning contribution is ~10 DU on average for much of the year and peaks in May, accounting for more than 60 % of the total TCO with 17 DU, and are directly responsible for the O_3 enhancement in May. Biomass burning has a rather small contribution during January to July. The significant biomass burning impact during September to November is associated with the 2006 fires in Equatorial Asia (Logan et al., 2008; Chandra et al., 2009; Nassar et al. 2009; Zhang et al., 2011). Lightning also makes a significant contribution to the September–November enhancement, as seen in Fig. 8 and was discussed in more detail by Zhang et al. (2011). Without any relative enhancement in May, however, stratospheric downward flux merely provides a background throughout the year. The contributions from soil and anthropogenic activities are negligibly small (less than 2.5 DU) throughout the year, and none of which peaks in May. Though the contribution from biogenic emission has a peak in May, the contribution is considerably smaller, too.

The relative contributions to the TCO over the ESIO from lightning NO_x emissions from the five regions (Fig. 1) are shown in Fig. 9 and summarized in Table 2. Lightning NO_x emissions from Equatorial Asia contribute ~4 to 5 DU to TCO from April to December 2006, with relative enhancements in May (29.2 % of the total lightning TCO, i.e., TCO resulting from lightning NO_x emissions) and October–November. Interestingly and somewhat surprisingly, the contributions to TCO from Central African and South American lightning NO_x emissions both show sharp peaks in May, ~3.5 DU (20.8 % of the total lightning TCO) for Central Africa and 3.0 DU (17.9 % of the total lightning TCO) for South America. We will discuss the lightning outflow from these two regions and its transport to the ESIO in subsequent sections. Figure 9a shows that lightning NO_x emissions from South Asia make relatively small contributions to the TCO enhancement in May (less than 1 DU or 4.8 %) and through much of the year, with a slight uptick during the summer months (~1 to 2 DU). The contribution from lightning

ACPD
12, 1979–2024, 2012

NO_x emissions from the tropical Indian Ocean is negligibly small (less than 0.5 DU or 2.4 %) all year long. Together, lightning NO_x emissions from the aforementioned five regions lead to 75.1 % of the total lightning TCO in May 2006 over the ESIO. Lightning NO_x emissions from the rest of the world contribute 5.4 % (0.9 DU). This contribution is comparable to that from South Asia lightning NO_x emissions in May and much smaller than those from the Equatorial Asia, Central Africa and South America. Without any relative enhancement in May, however, it decreases from April and merely provides a low background. The lightning NO_x emissions from the rest of the world contribute less than the remaining to the five subdomains reflects not only the nonlinearity both also the transport impacts. In effect, lightning NO_x emissions from Equatorial Asia, Central Africa and South America and subsequent O_3 production determine the O_3 maximum in May 2006. Overall, lightning TCO accounts for 61.8 % of the total TCO over the ESIO in May 2006, of which 18.0 %, 12.9 %, and 11.0 % are because of the lightning NO_x emissions from Equatorial Asia, Central Africa and South America, respectively (Fig. 9b and Table 2).

Figure 10 shows the vertical and longitudinal distributions of monthly average O_3 over 10° S-equator, resulting from lightning NO_x emissions from Equatorial Asia, Central Africa and South America in May 2006. The O_3 mixing ratios are averaged over the latitudinal range of each region. The two dashed lines indicate the longitudinal range of the ESIO. There is widespread Equatorial Asian lightning O_3 in the middle and upper troposphere over a broad swath between 60° E and 60° W longitudes, with peak O_3 mixing ratios (∼18 ppbv) at 200 to 300 hPa over the eastern ESIO (Fig. 10, top panel). A tongue of Equatorial Asian lightning O_3 extends down to the lower troposphere over the eastern ESIO because of intense deep convective activities in that region. Lightning O_3 from Central Africa makes a significant contribution to O_3 (6 to 12 ppbv) in the middle and upper troposphere over much of the ESIO, with peak values (12 ppbv) at 200 to 500 hPa over the western ESIO (Fig. 10, middle panel). The contribution from South American lightning O_3 (4 to 8 ppbv) is primarily in the middle to upper troposphere over the western ESIO (Fig. 10, bottom panel).

ACPD
12, 1979–2024, 2012

6 Interannual variability of tropospheric O_3 over the ESIO

6.1 Tropospheric O_3 over the ESIO from 2005 to 2009

We investigate in this section the interannual variability of the tropospheric O_3 over the ESIO. For this purpose we examined five years (2005 to 2009) of TES TCO and MLS upper tropospheric O_3 observations (Fig. 11). Relative enhancements of TCO are seen in May of 2006, 2007, 2008 and 2009 (no TES data for April through June 2005) in both TES observations and model results (Fig. 11a). The enhancements are pronounced and largest in May of 2006 and 2008 with TCO values over 30 DU. The enhancements in 2007 and 2009 extend from May through July and peak in June. Model results also capture the distinct relative enhancements during October–November 2006 that are related to the 2006 Indonesian fires (Zhang et al., 2011 and references therein) but completely miss those for 2007 and 2009 when model results are vastly lower than the observations in September-December. Overall, model simulated TCOs show seasonal variations that are broadly consistent with the observations for 2006 and 2008. Upper tropospheric O_3 at 215 hPa also show clear relative enhancements in May of 2006 and 2008, both in MLS observations and model results (Fig. 11b). Model results are generally lower by 20 ppbv than the observations, but MLS O_3 at 215 hPa is known to have a positive bias of ~20 ppbv (Livesey et al., 2008, 2011). Model results capture the seasonal cycles of O_3 observed by MLS.

Figure 12 compares GEOS-Chem simulated TCO with TCO from TES and total column O_3 from AIRS, OMI and TES. Model results from two simulations driven by GEOS-4 (2005 to 2006) and by GEOS-5 (2005 to 2009) meteorological data are shown. There are considerable differences among the total column O_3 from the three satellite data sets. The interannual variability of OMI total column O_3 correlates very well with that of TES, but much lower than TES. This has also been pointed out by previous study that TES is higher than OMI by 10 DU for the total column O_3 (Osterman et al., 2008). Most of the temporal variations of AIRS total column O_3 also follow those of TES and OMI. Other than the enhanced total column O_3 periods, AIRS total column O_3 is much

ACPD
12, 1979–2024, 2012

lower than those of TES and OMI during most of the periods. These differences may be due to sampling bias (e.g., AIRS am but TES/OMI pm). Our comparison between GEOS-Chem TCO and the satellite observed total column O_3 is qualitative rather than quantitative, and we focus on the temporal variability of O_3. Robust TCO and total column O_3 enhancements are seen in every May from 2005 to 2009 in both the observations and model results. Again, the observed total column O_3 enhancements are most distinct in May of 2006 and 2008 in AIRS, TES and OMI observations. The large O_3 enhancements during September-November 2006 are associated with the 2006 Indonesian fires (Logan et al., 2008; Chandra et al., 2009; Nassar et al. 2009; Zhang et al., 2011). Model simulations driven by GEOS-5 reanalysis reproduce the observed enhancements and the interannual variability.

6.2 Interannual variability of lightning O_3

We conducted model sensitivity simulations driven by GEOS-5 meteorological data for 2005–2009 to quantify the interannual lightning contributions to tropospheric O_3 over the ESIO by turning off lightning NO_x emissions. The results of total and lighting TCO and 215 hPa O_3 are shown in Fig. 13. Lightning NO_x emissions contribute to the peaks of O_3 in May every year for 2005 to 2009. The largest contributions to TCO are in 2006 and 2008 (Fig. 13a) and to O_3 (mixing ratios at 215 hPa are shown) in 2005, 2006 and 2008 (Fig. 13b). Lightning O_3 clearly controls the May enhancements. However, there is no apparent interannual variability in the model simulated lightning NO_x emissions from Equatorial Asia, Central Africa and South America – the emissions are not significantly larger in May of 2006 and 2008 than in the other three years (Fig. 14). There are clearly additional factors that drive the interannual variability of the tropospheric O_3 maximum in May over the ESIO.

ACPD
12, 1979–2024, 2012

6.3 Anti-cyclonic circulation of Central African and South American lightning outflow

We examine in this section the dynamics as a potential factor for determining the interannual variability of the tropospheric O_3 maximum in May over the ESIO. The lightning O_3 and flux from low troposphere to upper troposphere in May from 2005 to 2009 are investigated. The anti-cyclone is only shown in the middle troposphere (500 hPa) over the Southern Indian Ocean in May of 2006 and 2008 accompanied with high lightning O_3, even though the lightning O_3 is much higher in the upper troposphere. Figure 15 shows GEOS-Chem simulated monthly middle tropospheric (500 hPa) lightning O_3 and flux in May for 2005 to 2009. In the Southern Hemisphere, high lightning O_3 are widespread across the southern tropical Indian and South Atlantic Oceans, southern Africa and northern Australia, along the pathways of lightning outflow from Central Africa and South America. The lightning O_3 are much stronger in 2006 and 2008 than in 2005, 2008 and 2009. There are strong divergences and northward transport of lightning O_3 fluxes over the Southern Indian Ocean in 2006 and 2008. In effect, the anomalous anti-cyclonic circulations in May of 2006 and 2008 effectively entrain and transport O_3 in the African and South American lightning outflow to the ESIO. The divergence and northward transport are largely absent in the other three years. Figure 16 shows anomalies of 500 hPa winds based on 40 yr (1970–2009) of climatology from the National Center for Environmental Prediction/National Center for Atmospheric Research (NCEP/NCAR) reanalysis (Kalnay et al., 1996). Anomalous anti-cyclones and southerly winds are evident in May of 2006 and 2008, but not in the other three years. Figure 17 shows net O_3 productions at 500 hPa in May. The net O_3 productions are much larger in May of 2006 and 2008 than in May of 2005, 2007 and 2009. Therefore, the interannual variability of the May O_3 maximum is driven largely by the anomalous anti-cyclones over the southern Indian Ocean in May of 2006 and 2008.

ACPD
12, 1979–2024, 2012

A Tropospheric ozone maximum over the Indian Ocean

L. Zhang et al.

7 Summary and conclusions

We analyzed 5-yr (2005–2009) tropospheric O_3 observations over the Equatorial Southern Indian Ocean (ESIO) from satellite instruments MLS, TES, OMI, and AIRS, using the GEOS-Chem global three-dimensional chemical transport model. Model simulated upper tropospheric O_3 and tropospheric column O_3 (TCO) were compared against the observations. The effects of NO_x sources from lightning, biomass burning, soil, stratospheric downward transport, anthropogenic and biogenic emissions on the tropospheric O_3 over the ESIO, including the seasonal and interannual variability, were examined. In addition, we investigated the effects of dynamics on the interannual variability of tropospheric O_3 over the ESIO.

The satellite observations of tropospheric O_3 showed significant enhancements over the ESIO in May. The enhancements were evident not only in MLS upper tropospheric O_3, TES middle and upper tropospheric O_3 and TCO, but also in TES, OMI, and AIRS total column O_3. The enhancements were strongest in 2006 and 2008 and less pronounced in 2005, 2007 and 2009. GEOS-Chem simulations driven by GEOS-5 reanalysis data, with lightning flash rates parameterized based upon convective cloud top heights, were able to capture the May O_3 enhancements and the associated interannual variability.

We found that lightning contribution accounted for more than 60 % (17 DU) of the total TCO in May, and largely controlled the May O_3 enhancement. The lightning contribution was dominated by lightning NO_x emissions from Equatorial Asia, Central Africa and South America. Equatorial Asian lightning contributed on average ~4 to 5 DU (29.2 % of the total lightning TCO) to the TCO from April through December 2006, with clear enhancements in May. The contributions to the TCO from Central African (~3.5 DU, 20.8 %) and South American (~3.0 DU, 17.9 %) lightning NO_x emissions both showed distinct peaks in May. We found that NO_x emissions from biomass burning, soil, anthropogenic activities and biogenic sources had rather small contributions (less than 2.5 DU) to the tropospheric O_3 enhancements in May. The stratospheric downward transport provided a background about 5 DU throughout the year.

ACPD
12, 1979–2024, 2012

The larger and more distinct enhancements in May of 2006 and 2008 than those in May of 2005, 2007, and 2009 were a direct result of the anomalous anti-cyclonic circulations over the Southern Indian Ocean, which were much stronger in 2006 and 2008 than in the other three years. The anomalous anti-cyclonic circulation extended to the middle troposphere. The large-scale subsidence associated with the anti-cyclones served as a conduit that channeled downward the middle and upper tropospheric lightning outflow from Central Africa and South America. As such, lightning O_3 outflows from Central Africa and South America were effectively entrained by the anti-cyclones, followed by northward transport to the ESIO. Therefore, the interannual variability of the tropospheric O_3 enhancements over the ESIO was largely driven by these anomalous anti-cyclones over the Southern Indian Ocean.

Acknowledgements. This research was supported in part by NASA grants NNX09AF07G and NNX08AF64G from the Atmospheric Chemsitry Modeling and Analysis Program (ACMAP). We also acknowledge supports by the NASA Aura Science Team program. Work at Jet Propulsion Laboratory, California Institute of Technology was done under contract with the National Aeronautics and Space Administration. The GEOS-Chem model is managed by the Atmospheric Chemistry Modeling group at Harvard University with support from the NASA ACMAP program. We thank Jennifer Logan for helpful discussions.

References

Allen, D. J. and Pickering, K. E.: Evaluation of lightning flash rate parameterizations for use in a global chemical transport model, J. Geophys. Res., 107, 4711, doi:10.1029/2002JD002066, 2002.

Allen, D. J., Kasibhatla, P., Thompson, A. M., Rood, R. B., Doddridge, B. G., Pickering, K. E., Hudson, R. D., and Lin, S.-J.: Transport induced interannual variability of carbon monoxide using a chemistry and transport model, J. Geophys. Res., 101, 28655–28670, 1996a.

Allen, D. J., Rood, R. B., Thompson, A. M., and Hidson, R. D.: Three-dimensional 222Rn calculations using assimilated data and a convective mixing algorithm, J. Geophys. Res., 101, 6871–6881, 1996b.

Allen, D. J., Pickering, K. E., Stenchikov, G. L., Thompson, A. M., and Kondo, Y.: A three-dimensional total odd nitrogen (NO_y) simulation during SONEX using a stretched-grid chemical transport model, J. Geophys. Res., 105(D3), 3851-3876, 2000.

Allen, D. J., Pickering, K. E., Duncan, B., and Damon, M.: Impact of lightning NO emissions on North American photochemistry as determined using the Global Modeling Initiative (GMI) model, J. Geophys. Res., 115, D22301, doi:10.1029/2010JD014062, 2010.

Aumann, H. H., Chahine, M. T., Gautier, C., Goldberg, M. D., Kalnay, E., McMillin, L. M., Revercomb, H., Rosenkranz, P. W., Smith, W. L., Staelin, D. H., Strow, L. L., and Susskind, J.: AIRS/AMSU/HSB on the Aqua mission: Design, science objectives and data products, IEEE T. Geosci. Remote Sens., 41, 253–264, doi:10.1109/TGRS.2002.808356, 2003.

Balis, D., Kroon, M., Koukouli, M. E., Brinksma, E. J., Labow, G., Veefkind, J. P., and McPeters, R. D.: Validation of Ozone Monitoring Instrument total ozone column measurements using Brewer and Dobson spectrophotometer ground-based observations, J. Geophys. Res., 112, D24S46, doi:10.1029/2007JD008796, 2007.

Beer, R.: TES on the Aura mission: Scientific objectives, measurements, and analysis overview, IEEE T. Geosci. Remote Sens., 44, 1102–1105, doi:10.1109/TGRS.2005.863716, 2006.

Beer, R., Glavich, T. A., and Rider, D. M.: Tropospheric Emission Spectrometer for the Earth Observing System's Aura satellite, Appl. Opt., 40, 2356–2367, 2001.

Benkovitz, C., Scholtz, M., Pacyna, J., Tarrasón, L., Dignon, J., Voldner, E., Spiro, P., Logan, J., and Graedel, T.: Global gridded inventories of anthropogenic emissions of sulfur and nitrogen, J. Geophys. Res., 101, 29239–29253, 1996.

Bey, I., Jacob, D. J., Yantosca, R. M., Logan, J. A., Field, B. D., Fiore, A. M., Li, Q. B., Liu, H. G. Y., Mickley, L. J., and Schultz, M. G.: Global modeling of tropospheric chemistry with assimilated meteorology: Model description and evaluation, J. Geophys. Res., 106, 23073–23096, 2001.

Bowman, K. W., Rodgers, C. D., Kulawik, S. S., Worden, J., Sarkissian, E., Osterman, G., Steck, T., Luo, M., Eldering, A., Shephard, M., Worden, H., Lampel, M., Clough, S., Brown, P., Rinsland, C., Gunson, M., and Beer, R.: Tropospheric emission spectrometer: Retrieval method and error analysis, IEEE T. Geosci. Remote Sens., 44, 1297–1307, doi:10.1109/TGRS.2006.871234, 2006.

Brasseur, G. P., Hauglustaine, D. A., Walters, S., Rasch, P. J., Müller, J.-F., Granier, C., and Tie, X. X.: MOZART: A global chemical transport model for ozone and related chemical tracers:

1. Model description, J. Geophys. Res., 103, 28265–28289, 1998.
Chandra, S., Ziemke, J. R., Duncan, B. N., Diehl, T. L., Livesey, N. J., and Froidevaux, L.: Effects of the 2006 El Niño on tropospheric ozone and carbon monoxide: implications for dynamics and biomass burning, Atmos. Chem. Phys., 9, 4239–4249, doi:10.5194/acp-9-4239-2009, 2009.
Chen, Y., Li, Q., Randerson, J. T., Lyons, E. A., Kahn, R. A., Nelson, D. L., and Diner, D. J.: The sensitivity of CO and aerosol transport to the temporal and vertical distribution of North American boreal fire emissions, Atmos. Chem. Phys., 9, 6559–6580, doi:10.5194/acp-9-6559-2009, 2009.
Christian, H. J., Blakeslee, R. J., Boccippio, D. J., Boeck, W. L., Buechler, D. E., Driscoll, K. T., Goodman, S. J., Hall, J. M., Koshak, W. J., Mach, D. M., and Stewart, M. F.: Global frequency and distribution of lightning as observed from space by the optical transient detector, J. Geophys. Res., 108, 4005, doi:10.1029/2002JD002347, 2003.
Divakarla, M., Barnet, C., Goldverg, M., Maddy, E., Irion, F., Newchurch, M., Liu, X. P., Wolf, W., Flynn, L., Labow, G., Xiong, X. Z., Wei, J., and Zhou, L.: Evaluation of Atmospheric Infrared Sounder ozone profiles and total ozone retrievals with matched ozonesonde measurements, ECMWF ozone data, and Ozone Monitoring Instrument retrievals, J. Geophys. Res., 113, D15308, doi:10.1029/2007JD009317, 2008.
Fishman, J., C. Watson, E., Larsen, J. C., and Logan, J. A.: Distribution of tropospheric ozone determined from satellite data, J. Geophys. Res., 95, 3599–3617, 1990.
Giglio, L., Descloitres, J., Justice, C. O., and Kaufman, Y. J.: An enhanced contextual fire detection algorithm for MODIS, Remote Sens. Environ., 87, 273–282, 2003.
Giglio, L., van der Werf, G. R., Randerson, J. T., Collatz, G. J., and Kasibhatla, P.: Global estimation of burned area using MODIS active fire observations, Atmos. Chem. Phys., 6, 957–974, doi:10.5194/acp-6-957-2006, 2006.
Guenther, A., Karl, T., Harley, P., Wiedinmyer, C., Palmer, P. I., and Geron, C.: Estimates of global terrestrial isoprene emissions using MEGAN (Model of Emissions of Gases and Aerosols from Nature), Atmos. Chem. Phys., 6, 3181–3210, doi:10.5194/acp-6-3181-2006, 2006.
Hack, J. J.: Parameterization of moist convection in the NCAR community climate model (CCM2), J. Geophys. Res., 99, 5551–5568, doi:10.1029/93JD03478, 1994.
Hudman, R. C., Jacob, D. J., Turquety, S., Leibensperger, E. M., Murray, L. T., Wu, S., Gilliland, A. B., Avery, M., Bertram, T. H., Brune, W., Cohen, R. C., Dibb, J. E., Flocke, F. M., Fried,

ACPD
12, 1979–2024, 2012

A Tropospheric ozone maximum over the Indian Ocean

L. Zhang et al.

A., Holloway, J., Neuman, J. A., Orville, R., Perring, A., Ren, X., Sachse, G. W., Singh, H. B., Swanson, A., and Wooldridge, P. J.: Surface and lightning sources of nitrogen oxides over the United States: Magnitudes, chemical evolution, and outflow, J. Geophys. Res., 112, D12S05, doi:10.1029/2006JD007912, 2007.

Jacob, D. J., Heikes, B. G., Fan, S.-M., Logan, J. A., Mauzerall, D. L., Bradshaw, J. D., Singh, H. B., Gregory, G. L., Talbot, R. W., Blake, D. R., and Sachse, G. W.: Origin of ozone and NO_x in the tropical troposphere: a photochemical analysis of aircraft observations over the South Atlantic Basin, J. Geophys. Res., 101, 24235–24350, 1996.

Jourdain, L., Worden, H. M., Bowman, K., Li, Q. B., Eldering, A., Kulawik, S. S., Osterman, G., Boersma, K. F., Fisher, B., Rinsland, C. P., Beer, R., and Gunson, M.: Tropospheric vertical distribution of tropical Atlantic ozone observed by TES during the northern African biomass burning season, Geophys. Res. Lett., 34, L04810, doi:10.1029/2006GL028284, 2007.

Jourdain, L., Kulawik, S. S., Worden, H. M., Pickering, K. E., Worden, J., and Thompson, A. M.: Lightning NO_x emissions over the USA constrained by TES ozone observations and the GEOS-Chem model, Atmos. Chem. Phys., 10, 107–119, doi:10.5194/acp-10-107-2010, 2010.

Kalnay E., Kanamitsu, M., Kistler, R., Collins, W., Deaven, D., Gandin, L., Iredell, M., Saha, S., White, G., Woollen, J., Zhu, Y., Leetmaa, A., Reynolds, B., Chelliah, M., Ebisuzaki, W., Higgins, W., Janowiak, J., Mo, K. C., Ropelewski, C., Wang, J., Jenne, R., and Joseph, D.: The NCEP/NCAR 40-year reanalysis project, B. Am. Meteor. Soc., 77, 437–471, 1996.

Komala, N., Saraspriya, S., Kita, K., and Ogawa, T.: Tropospheric ozone behavior observed in Indonesia, Atmos. Environ., 30, 1851–1856, 1996.

Kulawik, S. S., Worden, J., Eldering, A., Bowman, K., Gunson, M., Osterman, G. B., Zhang, L., Clough, S., Shephard, M. W., and Beer, R.: Implementation of cloud retrievals for Tropospheric Emission Spectrometer (TES) atmospheric retrievals: part 1. Description and characterization of errors on trace gas retrievals, J. Geophys. Res., 111, D24204, doi:10.1029/2005JD006733, 2006.

Lacis, A. A., Wuebbles, D. J., and Logan, J. A.: Radiative forcing of climate by changes in the vertical distribution of ozone, J. Geophys. Res., 95, 9971–9981, doi:10.1029/JD095iD07p09971, 1990.

Levelt, P. F., van den Oord, G. H. J., Dobber, M. R., Mälkki, A., Visser, H., de Vries, J., Stammes, P., Lundell, J. O. V., and Saari, H.: The Ozone Monitoring Instrument, IEEE T. Geosci. Remote Sens., 44, 1093–1101, doi:10.1109/TGRS.2006.872333, 2006a.

Levelt, P. F., Hilsenrath, E., Leppelmeier, G. W., van den Oord, G. H. J., Bhartia, P. K., Tamminen, J., de Haan, J. F., and Veefkind, J. P.: Science objectives of the Ozone Monitoring Instrument, IEEE T. Geosci. Remote Sens., 44, 1199–1208, doi:10.1109/TGRS.2006.872336, 2006b.

Levy, H.: Normal atmosphere: Large radical and formaldehyde concentrations predicted, Science, 173, 141–143, 1971.

Lin, S. J. and Rood, R. B.: Multidimensional flux form semi-Lagrangian transport schemes, Mon. Weather Rev., 124, 2046–2070, 1996.

Livesey, N. J., Snyder, W. V., Read, W. G., and Wagner, P. A.: Retrieval algorithms for the EOS Microwave Limb Sounder (MLS) instrument, IEEE T. Geosci. Remote Sens., 44, 1144–1155, 2006.

Livesey, N. J., Filipiak, M., Froidevaux, L., Read, W., Lambert, A., Santee, M., Jiang, J., Waters, J., Drouin, B., Cofield, R., Cuddy, D., Fuller, R., Jarnot, R., Jiang, Y., Knosp, B., Li, Q. B., Schwartz, M., Snyder, W., Stek, P., Wagner, P., Pumphrey, H., Avery, M., Browell, E., Christiensen, L., Edwards, D., Emmons, L., Fahey, D., Gao, R., Loewenstein, M., Lopez, J., Osterman, G., Sachse, G., and Webster, C.: Validation of EOS MLS O_3 and CO observations in the upper troposphere and lower stratosphere, J. Geophys. Res., 113, D15S02, doi:10.1029/2007JD008805, 2008.

Livesey, N. J., Read, G. W., Froidevaux, L., Lambert, A., Manney, L. G., Pumphrey, C. H., Santee, L. M., Schwartz, J. M., Wang, S., Cofield, E. R., Cuddy, T. D., Fuller A. R., Jarnot, F. R., Jiang, H. J., Knosp, W. B., Stek C. P., Wagner, A. P., and Wu L. D.: Version 3.3 Level 2 data quality and description document, Jet Propulsion Laboratory, 2011.

Logan, J. A., Prather, M. J., Wofsy, S. C., and McElroy, M. B.: Tropospheric chemistry: A global perspective, J. Geophys. Res., 86, 7210–7254, 1981.

Logan, J. A., Megretskaia, I., Nassar, R., Murray, T. L., Zhang, L., Bowman, W. K., Worden, W. H., and Luo, M.: Effects of the 2006 El Niño on tropospheric composition as revealed by data from the Tropospheric Emission Spectrometer (TES), Geophys. Res. Lett., 35, L03816, doi:10.1029/2007GL031698, 2008.

Luo, M., Rinsland, C. P., Logan, J. A., Worden, J., Kulawik, S., Eldering, A., Goldman, A., Shephard, M. W., Gunson, M., and Lampel M.: Comparison of carbon monoxide measurements by TES and MOPITT: The influence of a priori data and instrument characteristics on nadir atmospheric species retrievals, J. Geophys. Res., 112, D09303, doi:10.1029/2006JD007663, 2007.

ACPD
12, 1979–2024, 2012

A Tropospheric ozone maximum over the Indian Ocean

L. Zhang et al.

Martin, R. V., Sauvage, B., Folkins, I., Sioris, C. E., Boone, C., Bernath, P., and Ziemke, J.: Space-based constraints on the production of nitric oxide by lightning, J. Geophys. Res., 112, D09309, doi:10.1029/2006JD007831, 2007.
McLinden, C. A., Olsen, S. C., Hannegan, B., Wild, O., Prather, M. J., and Sundet, J.: Stratospheric ozone in 3-D models: A simple chemistry and the cross-tropopause flux, J. Geophys. Res., 105, 14653–14666, 2000.
McPeters, R., Kroon, M., Labow, G., Brinksma, E., Balis, D., Petropavlovskikh, I., Veefkind, J. P., Bhartia, P. K., and Levelt, P. F.: Validation of the Aura Ozone Monitoring Instrument total column ozone product, J. Geophys. Res., 113, D15S14, doi:10.1029/2007JD008802, 2008.
Moorthi, S. and Suarez, M. J.: Relaxed Arakawa–Schubert: A parameterization of moist convection for general circulation models, Mon. Weather Rev., 120, 978–1002, 1992.
Murray, L. T., Logan, J. A., Jacob, D. J., and Hudman, R. C.: Spatial and interannual variability in lightning constrained by LIS/OTD satellite data for 1998–2006: implications for tropospheric ozone and OH, in preparation, 2012.
Nassar, R., Logan, J. A., Worden, H. M., Megretskaia, I. A., Bowman, K. W., Osterman, G. B., Thompson, A. M., Tarasick, D. W., Austin S., Claude, H., Dubey, M. K., Hocking, W. K., Johnson, B. J., Joseph, E., Merrill, J., Morris, G. A., Newchurch, M., Oltmans, S. J., Posny, F., Schmidlin, F. J., Vomel, H., Whiteman, D. N., and Witte, J. C.: Validation of Tropospheric Emission Spectrometer (TES) nadir ozone profiles using ozonesonde measurements, J. Geophys. Res., 113, D15S17, doi:10.1029/2007JD008819, 2008.
Nassar, R., Logan, J. A., Megretskaia, I. A., Murray, L. T., Zhang, L., and Jones, D. B. A.: Analysis of tropospheric ozone, carbon monoxide and water vapor during the 2006 El Niño using TES observations and the GEOS-Chem model, J. Geophys. Res., 114, D17304, doi:10.1029/2009JD011760, 2009.
Olivier, J. G. J. and Berdowski, J. J. M.: Global emissions sources and sinks, in: The Climate System, edited by: Berdowski, J., Guicherit, R., and Heij, B. J., 33–78, A. A. Balkema, Lisse, Netherlands, 2001.
Oman, L. D., Ziemke, J. R., Douglass, A. R., Waugh, D. W., Lang, C., Rodriguez, J. M., and Nielsen, J. E.: The response of tropical tropospheric ozone to ENSO, Geophys. Res. Lett., 38, L13706, doi:10.1029/2011GL047865, 2011.
Osterman, G. B., Kulawik, S. S., Worden, H., Richards, N. A., Fisher, B. M., Eldering, A., Shephard, M. W., Froidevaux, L., Labow, G., Luo, M., Herman, R. L., Bowman, K. W., and Thompson, A. M.: Validation of Tropospheric Emission Spectrometer (TES) measurements

ACPD
12, 1979–2024, 2012

of the total, stratospheric, and tropospheric column abundance of ozone, J. Geophys. Res., 113, D15S16, doi:10.1029/2007JD008801, 2008.
Parkinson, C. L.: Aqua: An Earth-observing satellite mission to examine waterand other climate variables, IEEE T. Geosci. Remote Sens., 41, 173–183, doi:10.1109/TGRS.2002.808319, 2003.
Pickering, K. E., Wang, Y. S., Tao, W. K., Price, C., and Muller, J. F.: Vertical distributions of lightning NO_x for use in regional and global chemical transport models, J. Geophys. Res., 103, 31203–31216, 1998.
Price, C. and Rind, D. H.: A simple lightning parameterization for calculating global lightning distributions, J. Geophys. Res., 97, 9919–9933, 1992.
Price, C. and Rind, D. H.: What determines the cloud-to-ground lightning fraction in thunderstorms?, Geophys. Res. Lett., 20, 463–466, 1993.
Price, C. and Rind, D. H.: Modeling global lightning distributions in a general circulation model, Mon. Weather Rev., 122, 1930–1939, 1994.
Randerson, J. T., Liu, H., Flanner, M. G., Chambers, S. D., Jin, Y., Hess, P. G., Pfister, G., Mack, M. C., Treseder, K. K., Welp, L. R., Chapin, F. S., Harden, J. W., Goulden, M. L., Lyons, E., Neff, J. C., Schuur, E., and Zender, C. S.: The impact of boreal forest fire on climate warming, Science, 314, 1130–1132, 2006.
Sander, S. P., Friedl, R. R., DeMore, W. B., Golden, D. M., Kurylo, M. J., Hampson, R. F., Huie, R. E., Moortgat, G. K., Ravishankara, A. R., Kolb, C. E., and Molina, M. J.: Chemical Kinetics and Photochemical Data for Use in Stratospheric Modeling, Technical Report JPL Publication 00-3, Jet Propulsion Laboratory, Pasadena, CA, 2000.
Sauvage, B., Martin, R. V., van Donkelaar, A., Liu, X., Chance, K., Jaeglé, L., Palmer, P. I., Wu, S., and Fu, T.-M.: Remote sensed and in situ constraints on processes affecting tropical tropospheric ozone, Atmos. Chem. Phys., 7, 815–838, doi:10.5194/acp-7-815-2007, 2007.
Schoeberl, M. R., Douglass, A. R., Hilsenrath, E., Bhartia, P. K., Beer, R., Waters, J. W., Gunson, M. R., Froidevaux, L., Gille, J. C., Barnett, J. J., Levelt, P. F., and DeCola, P.: Overview of the EOS Aura mission, IEEE T. Geosci. Remote Sens., 44, 1066–1074, doi:10.1109/TGRS.2005.861950, 2006.
Shim, C., Li, Q. B., Luo, M., Kulawik, S., Worden, H., Worden, J., Eldering, A., Avery, M., Diskin, G., Sachse, G., Weinheimer, A., Knapp, D., Montzca, D., and Campos, T.: Satellite observations of Mexico City pollution outflow from the Tropospheric Emissions Spectrometer (TES), Atmos. Environ., 43, 1540–1547, doi:10.1016/j.atmosenv.2008.11.026, 2009.

ACPD
12, 1979–2024, 2012

A Tropospheric ozone maximum over the Indian Ocean

L. Zhang et al.

Thompson, A. M., Witte, J. C., Hudson, R. D., Guo, H., Herman, J. R., and Fujiwara, M.: Tropical tropospheric ozone and biomass burning, Science, 291, 2128–2132, doi:10.1126/science.291.5511.2128, 2001.

van der Werf, G. R., Randerson, J. T., Giglio, L., Collatz, G. J., Kasibhatla, P. S., and Arellano Jr., A. F.: Interannual variability in global biomass burning emissions from 1997 to 2004, Atmos. Chem. Phys., 6, 3423–3441, doi:10.5194/acp-6-3423-2006, 2006.

Wang, Y., Jacob, D. J., and Logan, J. A.: Global simulation of tropospheric O_3-NO_x-hydrocarbon chemistry, 1. Model formulation, J. Geophys. Res., 103, 10713–10726, 1998.

Waters, J. W., Froidevaux, L., Harwood, R. S., Jarnot, R. F., Pickett, H. M., Read, W. G., Siegel, P. H., Cofield, R. E., Filipiak, M. J., Flower, D. A., Holden, J. R., Lau, G. K., Livesey, N. J., Manney, G. L., Pumphrey, H. C., Santee, M. L., Wu, D. L., Cuddy, D. T., Lay, R. R., Loo, M. S., Perun, V. S., Schwartz, M. J., Stek, P. C., Thurstans, R. P., Boyles, M. A., Chandra, K. M., Chavez, M. C., Chen, G. S., Chudasama, B. V., Dodge, R., Fuller, R. A., Girard, M. A., Jiang, J. H., Jiang Y. Knosp, B. W., LaBelle, R. C., Lam, J. C., Lee, K. A., Miller, D., Oswald, J. E., Patel, N. C., Pukala, D. M., Quintero, O., Scaff, D. M., Van Snyder, W., Tope, M. C., Wagner, P. A., and Walch, M. J.: The Earth Observing System Microwave Limb Sounder (EOS MLS) on the Aura satellite, IEEE T. Geosci. Remote Sens., 44, 1075–1092, doi:10.1109/TGRS.2006.873771, 2006.

Wild, O., Zhu, X., and Prather, M. J.: FAST-J: Accurate simulation of in- and below-cloud photolysis in tropospheric chemical models, J. Atmos. Chem., 37, 245–282, 2000.

Worden, H. M., Logan, J. A., Worden, J. R., Beer, R., Bowman, K., Clough, S. A., Eldering, A., Fisher, B. M., Gunson, M. R., Herman, R. L., Kulawik, S. S., Lampel, M. C., Luo, M., Meqretskaia, I. A., Osterman, G. B., and Shephard, M. W.: Comparisons of Tropospheric Emission Spectrometer (TES) ozone profiles to ozonesondes: Methods and initial results, J. Geophys. Res., 112, D03309, doi:10.1029/2006JD007258, 2007.

Yevich, R. and Logan J. A.: An assessment of biofuel use and burning of agricultural waste in the developing world, Global Biogeochem. Cy., 17, 1095, doi:10.1029/2002GB001952, 2003.

Zhang, G. J. and McFarlane, N. A.: Sensitivity of climate simulations to the parameterization of cumulus convection in the Canadian climate centre general circulation model, Atmos.-Ocean, 33, 407–446, 1995.

Zhang, L., Li, Q. B., Jin, J., Liu, H., Livesey, N., Jiang, J. H., Mao, Y., Chen, D., Luo, M., and Chen, Y.: Impacts of 2006 Indonesian fires and dynamics on tropical upper tropospheric

ACPD
12, 1979–2024, 2012

Title Page
Abstract | Introduction
Conclusions | References
Tables | Figures
◀| |▶
◀ ▶
Back | Close
Full Screen / Esc
Printer-friendly Version
Interactive Discussion

carbon monoxide and ozone, Atmos. Chem. Phys., 11, 10929–10946, doi:10.5194/acp-11-10929-2011, 2011.
Zhang, Q., Streets, D. G., Carmichael, G. R., He, K. B., Huo, H., Kannari, A., Klimont, Z., Park, I. S., Reddy, S., Fu, J. S., Chen, D., Duan, L., Lei, Y., Wang, L. T., and Yao, Z. L.: Asian emissions in 2006 for the NASA INTEX-B mission, Atmos. Chem. Phys., 9, 5131–5153, doi:10.5194/acp-9-5131-2009, 2009.
Ziemke, J. R., Chandra, S., Duncan, B. N., Schoeberl, M. R., Torres, O., Damon, M. R., and Bhartia, P. K.: Recent biomass burning in the tropics and related changes in tropospheric ozone, Geophys. Res. Lett., 36, L15819, doi:10.1029/2009GL039303, 2009.

ACPD
12, 1979–2024, 2012

A Tropospheric ozone maximum over the Indian Ocean

L. Zhang et al.

Table 1. Description of model simulations.

Experiment	Year	Meteorological data	Lightning parameterization
A1	2006	GEOS-4	Convective cloud-top-height
A2	2006	GEOS-4	Convective cloud-top-height with local redistribution
A3	2005	GEOS-4	Convective mass flux
A4	2006	GEOS-4	Convective precipitation
B1	2006	GEOS-5	Convective cloud-top-height
B2	2006	GEOS-5	Convective cloud-top-height with local redistribution

ACPD
12, 1979–2024, 2012

Table 2. GEOS-Chem simulated total and lightning tropospheric column O_3 over the Equatorial Southern Indian Ocean (see Fig. 1). Values are monthly averages for May 2006.

Monthly total TCO over ESIO = 27.2 [DU], May 2006					
Total lightning contribution = 16.8 [DU] (61.8 %)					
Regional lightning contribution					
Equatorial Asia	Central Africa	South America	South Asia	Tropical Indian Ocean	Rest of the world
4.9 [DU] (18.0 %)	3.5 [DU] (12.9 %)	3.0 [DU] (11.0 %)	0.8 [DU] (3.0 %)	0.4 [DU] (1.5 %)	0.9 [DU] (3.3 %)
Percentage of total lightning contribution from regional lightning					
29.2 %	20.8 %	17.9 %	4.8 %	2.4 %	5.4 %

Discussion Paper | Discussion Paper | Discussion Paper | Discussion Paper |
ACPD
12, 1979–2024, 2012

A Tropospheric ozone maximum over the Indian Ocean

L. Zhang et al.

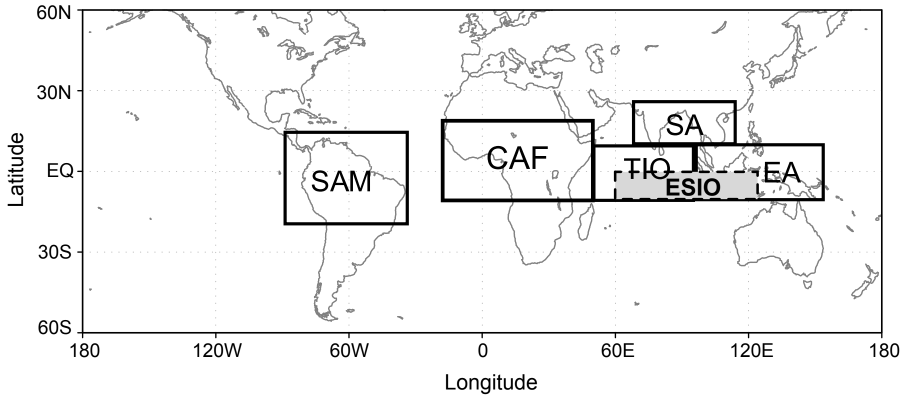

Fig. 1. The Equatorial Southern Indian Ocean (ESIO, 10° S–equator, 60° E–125° E; shaded area) and five tropical lightning regions: the tropical Indian Ocean (TIO: 10° S–10° N, 40° E–95° E), South Asia (SA: 10° N–30° N, 70° E–110° E), Equatorial Asia (EA: 10° S–10° N, 95° E–150° E), Central Africa (CA: 10° S–20° N, 20° W–40° E) and South America (SAM: 20° S–15° N, 85° W–35° W).

ACPD
12, 1979–2024, 2012

A Tropospheric ozone maximum over the Indian Ocean

L. Zhang et al.

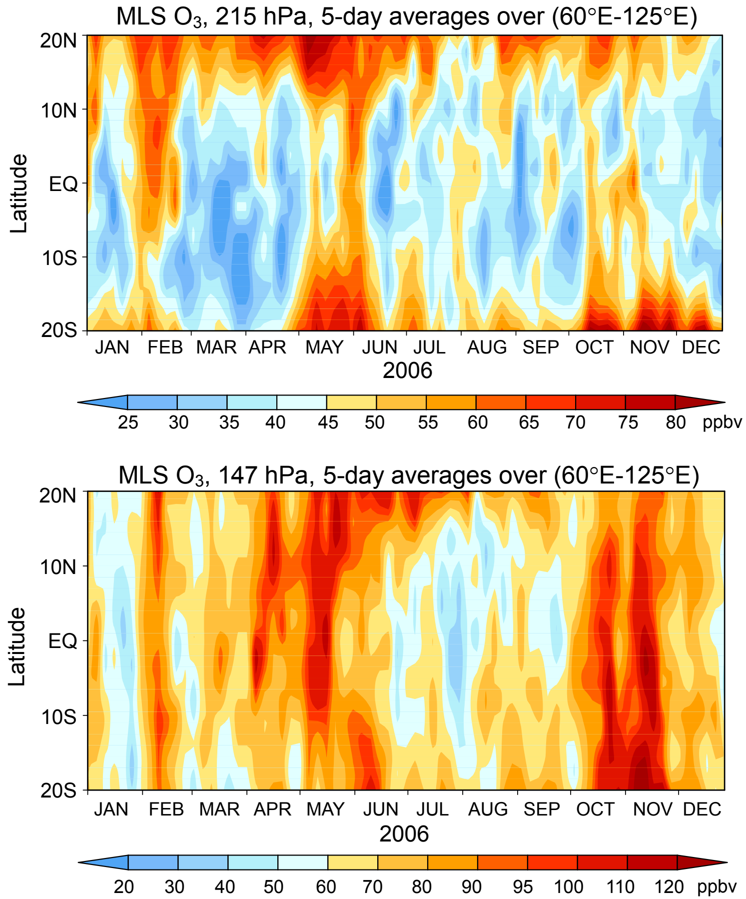

Fig. 2. MLS observed upper tropospheric O_3 at (top panel) 215 hPa and (bottom panel) 147 hPa over 20° S–20° N for 2006. Values are 5-day averages over the 60° E–125° E longitudes.

ACPD
12, 1979–2024, 2012

A Tropospheric ozone maximum over the Indian Ocean

L. Zhang et al.

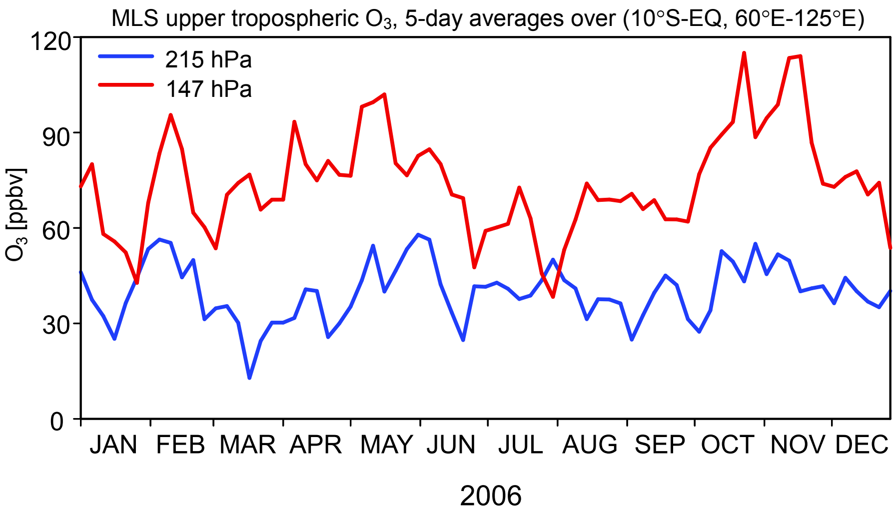

Fig. 3. MLS O_3 at 147 (red line) and 215 hPa (blue line), averaged over the Equatorial Southern Indian Ocean (see Fig. 1) for 2006. Values are 5-day averages.

ACPD
12, 1979–2024, 2012

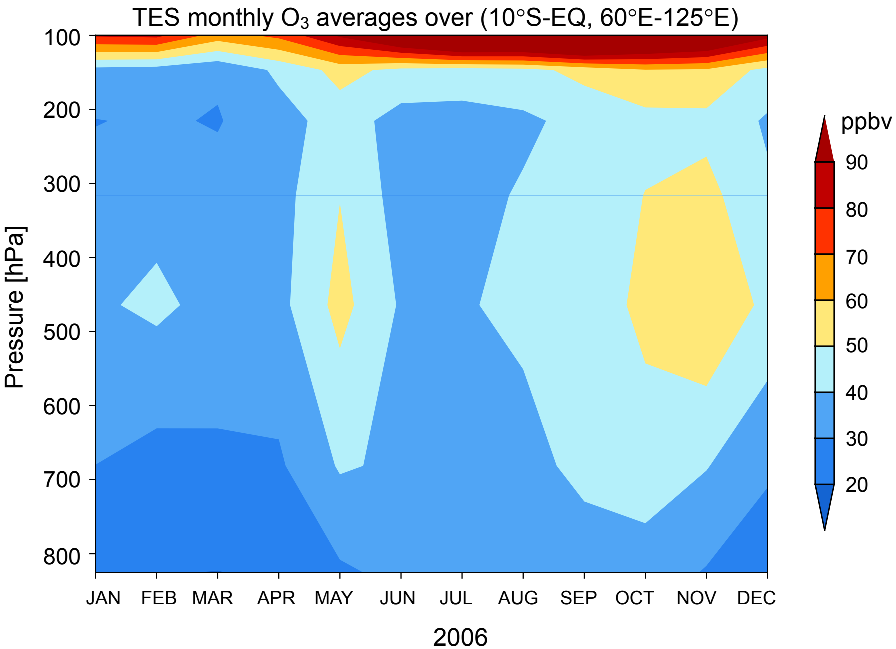

Fig. 4. TES tropospheric O_3 vertical distribution averaged over the Equatorial Southern Indian Ocean (see Fig. 1). Values are monthly means for 2006.

ACPD
12, 1979–2024, 2012

A Tropospheric ozone maximum over the Indian Ocean

L. Zhang et al.

Title Page
Abstract | Introduction
Conclusions | References
Tables | Figures
◀| |▶
◀ ▶
Back | Close
Full Screen / Esc
Printer-friendly Version
Interactive Discussion

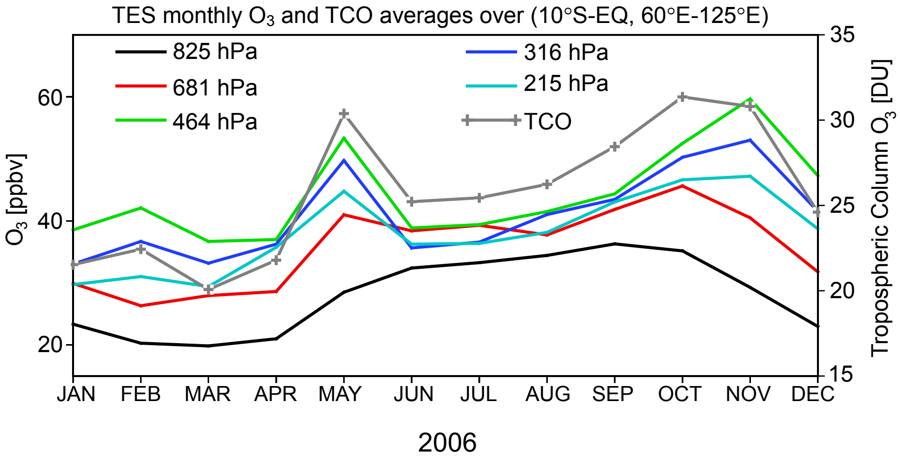

Fig. 5. TES tropospheric O_3 and tropospheric column O_3 (TCO) over the Equatorial Southern Indian Ocean (see Fig. 1). Values are monthly means for 2006.

Discussion Paper | Discussion Paper | Discussion Paper | Discussion Paper |

ACPD

12, 1979–2024, 2012

A Tropospheric ozone maximum over the Indian Ocean

L. Zhang et al.

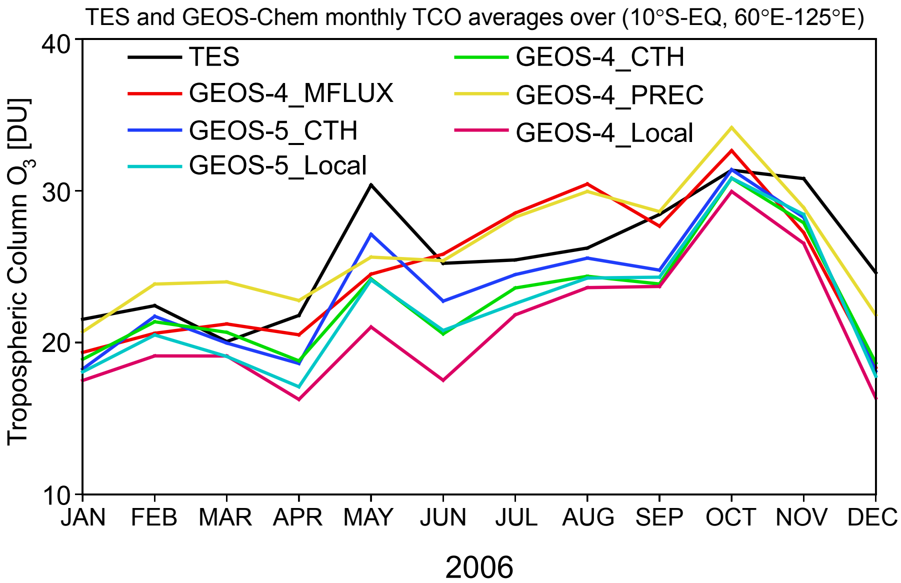

Fig. 6. TES retrieved and GEOS-Chem simulated monthly mean tropospheric column O_3 (TCO) for 2006 over the Equatorial Southern Indian Ocean (see Fig. 1). Model results from simulations driven by GEOS-4 and by GEOS-5 reanalysis data and with different lightning parameterizations are shown. See text for more detail.

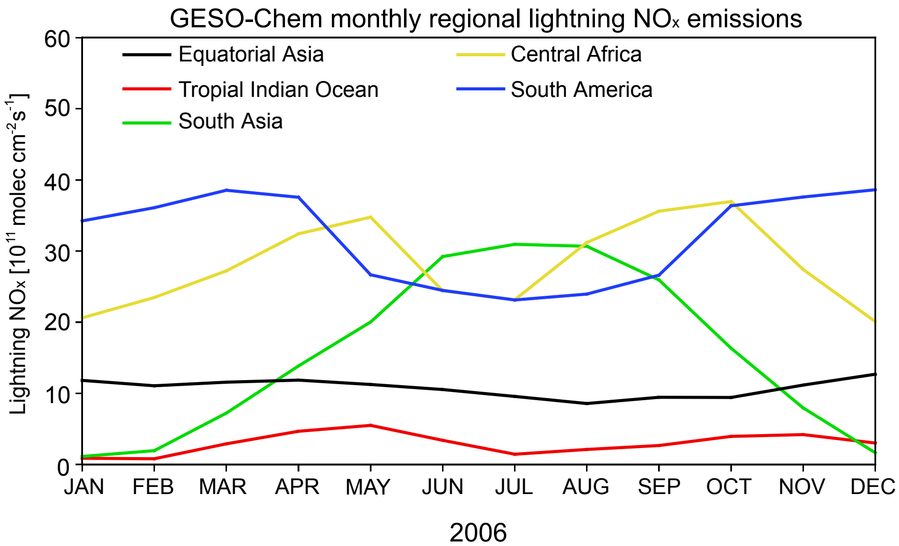

Fig. 7. GEOS-Chem simulated lightning NO_x emissions over Equatorial Asia (black line), Central Africa (yellow line), South America (blue line), South Asia, and the tropical Indian Ocean (red line). Values are monthly means for 2006. See Fig. 1 for domain definitions.

ACPD
12, 1979–2024, 2012

A Tropospheric ozone maximum over the Indian Ocean

L. Zhang et al.

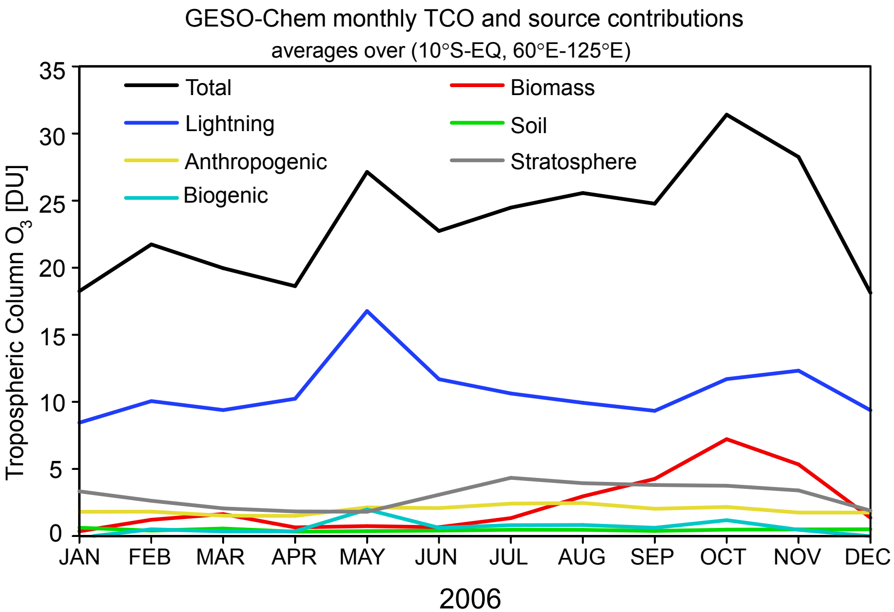

Fig. 8. GEOS-Chem simulated tropospheric column O_3 over the Equatorial Southern Indian Ocean (see Fig. 1). Values are monthly means for 2006. Also shown are tropospheric column O_3 because of NO_x emissions from lightning (blue line), biomass burning (red line), soil (green line), stratospheric downward transport (grey line), anthropogenic sources (yellow line), and biogenic sources(cyan line).

ACPD
12, 1979–2024, 2012
A Tropospheric ozone maximum over the Indian Ocean
L. Zhang et al.

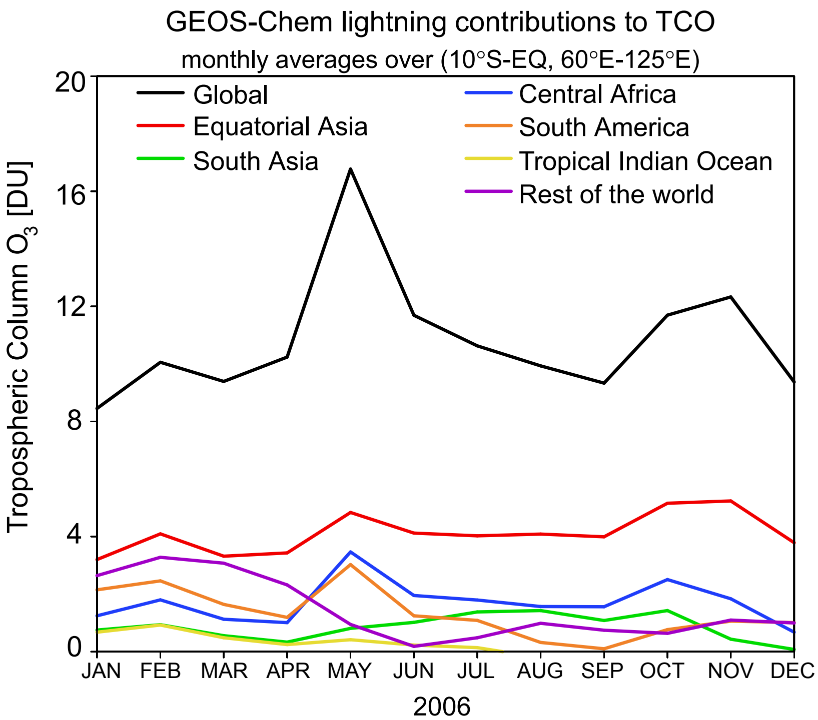

Fig. 9. GEOS-Chem simulated total and lightning tropospheric column O_3 over the Equatorial Southern Indian Ocean (see Fig. 1). Lightning O_3 refers to O_3 produced as a result of lightning NO_x emissions. Values are monthly means for 2006. Tropospheric column O_3 from lightning NO_x emissions over Equatorial Asia, Central Africa, South America, South Asia, and the tropical Indian Ocean (see Fig. 1) are shown.

ACPD
12, 1979–2024, 2012

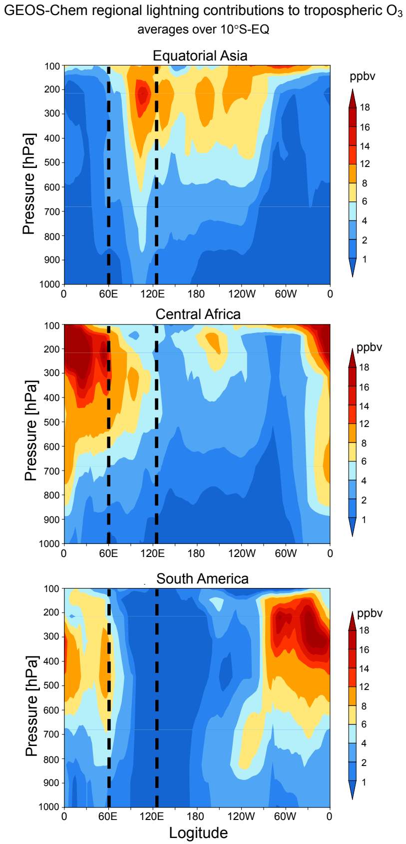

Fig. 10. GEOS-Chem simulated vertical and longitudinal distributions of tropospheric O_3 from Lightning NO_x emissions from (top panel) Equatorial Asia, (middle panel) central Africa, and (bottom panel) South America. Values are monthly means for May 2006, averaged over 10° S to the equator.

ACPD
12, 1979–2024, 2012

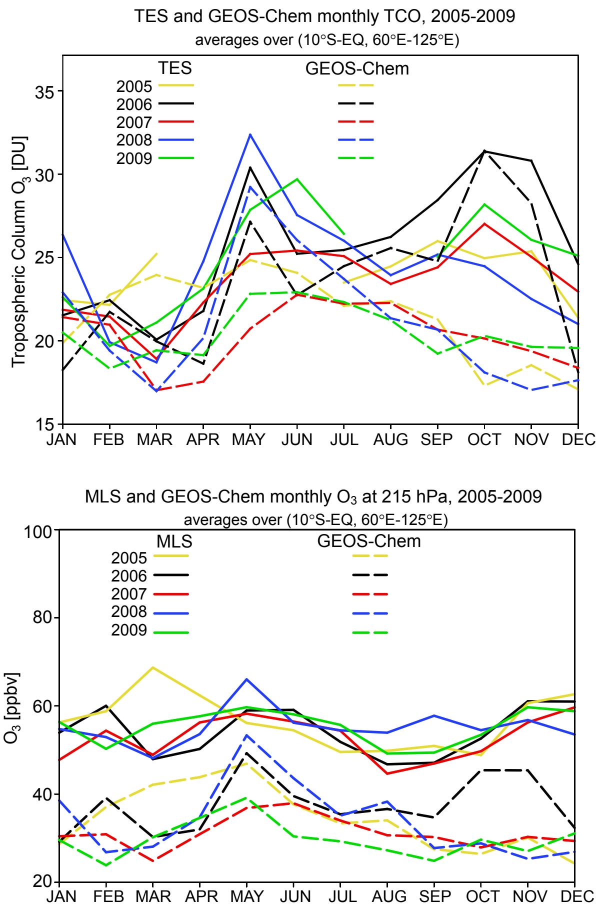

Fig. 11. Observed and simulated tropospheric column O_3 (top panel: TES – solid lines; GESO-Chem – dashed lines) and 215 hPa O_3 (bottom panel: MLS – solid lines; GESO-Chem – dashed lines) over the Equatorial Southern Indian Ocean (see Fig. 1). Values are monthly averages for 2005 to 2009.

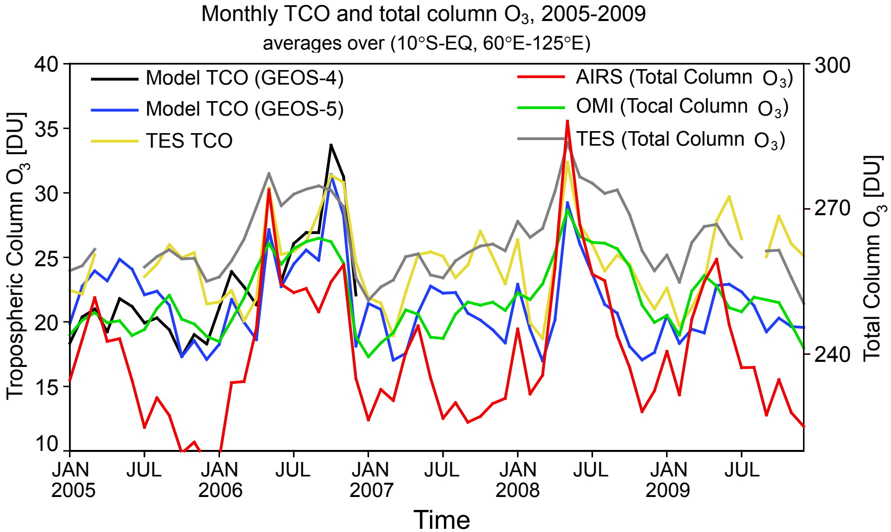

Fig. 12. Monthly mean tropospheric column O_3 from GEOS-Chem (black and blue lines) and TES (yellow line) and total column O_3 from AIRS (red line), OMI (green line) and TES (grey line) over the Equatorial Southern Indian Ocean (see Fig. 1) for 2005 to 2009. Results from model simulations driven by GEOS-4 (black line) and GEOS-5 (blue) reanalysis data are both shown. See text for more detail.

ACPD
12, 1979–2024, 2012

A Tropospheric ozone maximum over the Indian Ocean

L. Zhang et al.

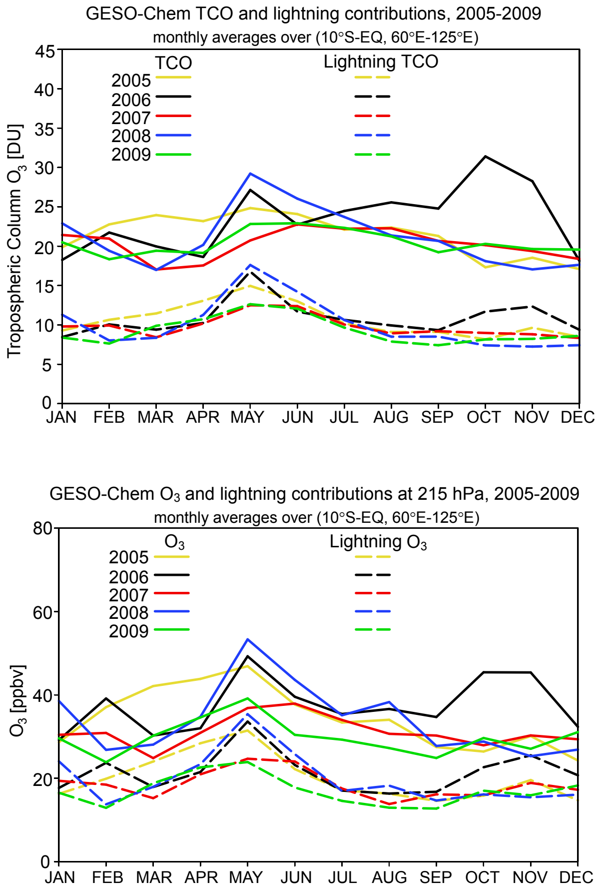

Fig. 13. GEOS-Chem simulated total and lightning tropospheric column O_3 (top panel) and 215 hPa total and lightning O_3 (bottom panel) over the Equatorial Southern Indian Ocean (see Fig. 1). Lightning O_3 refers to O_3 produced as a result of lightning NO_x emissions. Values are monthly means for 2005 to 2009.

ACPD
12, 1979–2024, 2012

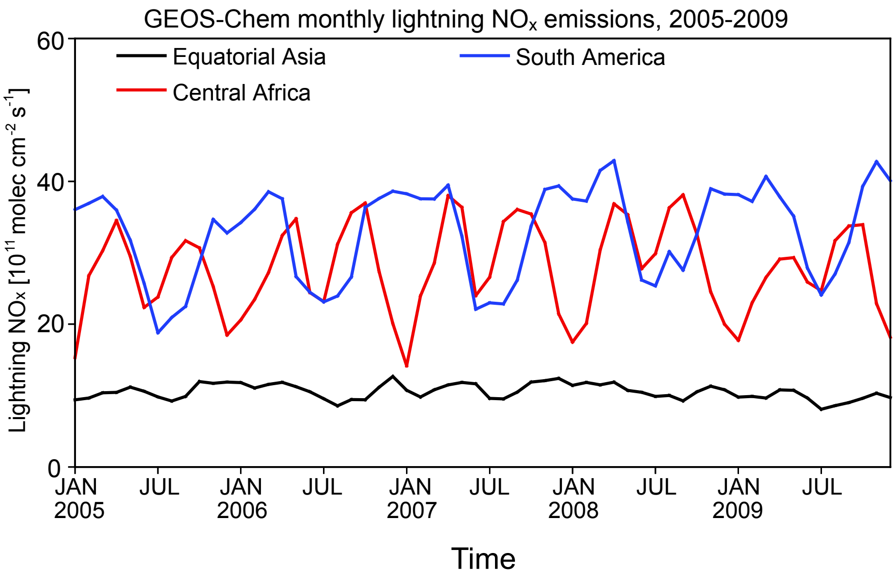

Fig. 14. GEOS-Chem simulated lightning NO_x emissions over Equatorial Asia, Central Africa, and South America (see Fig. 1). Values are monthly means for 2005 to 2009.

ACPD
12, 1979–2024, 2012

A Tropospheric ozone maximum over the Indian Ocean

L. Zhang et al.

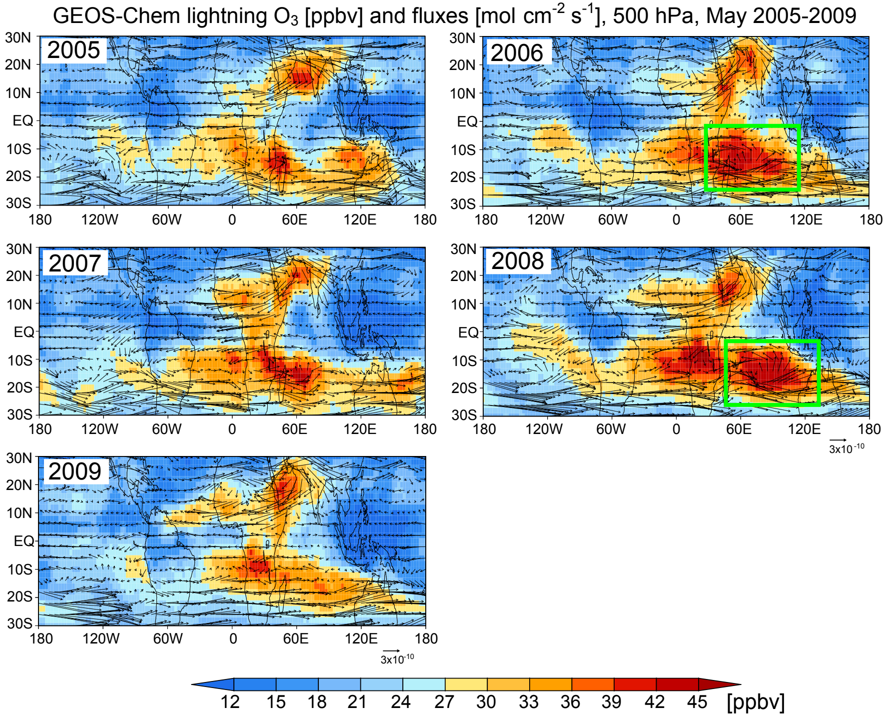

Fig. 15. GEOS-Chem simulated lightning O_3 concentrations (color contours, ppbv) and horizontal fluxes (arrows, mol cm^{-2} s^{-1}) at 500 hPa. Lightning O_3 refers to O_3 produced as a result of lightning NO_x emissions. Values are monthly means for May 2005 through 2009. Rectangles indicate regions of anomalous anti-cyclones.

ACPD
12, 1979–2024, 2012

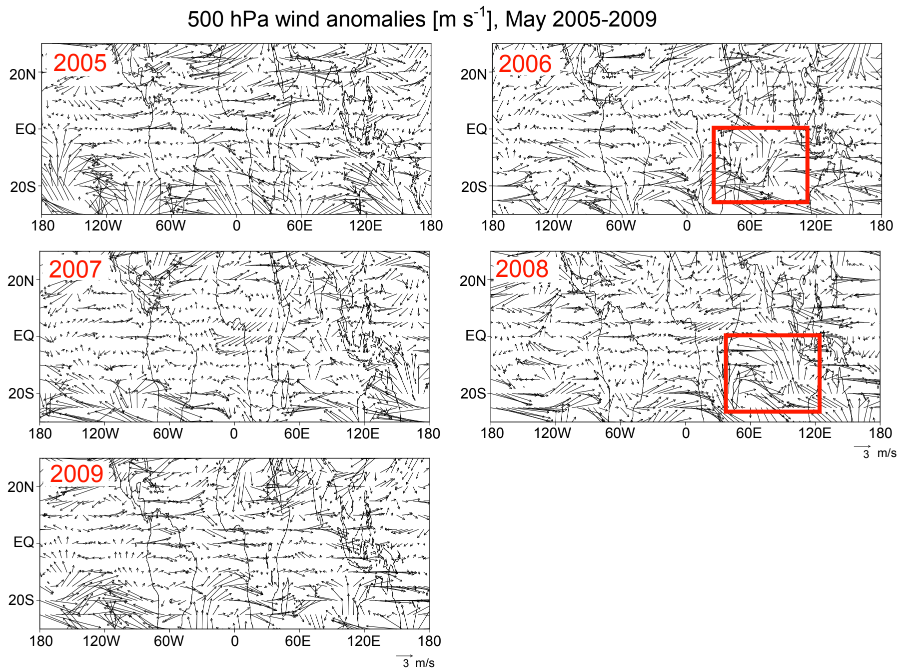

Fig. 16. Monthly mean NCEP wind anomalies ($m\,s^{-1}$) at 500 hPa for May of 2005 through 2009. NCEP reanalysis data provided by the NOAA/OAR/ESRL PSD, Boulder, Colorado, USA, from their web site at http://www.esrl.noaa.gov/psd/. Red rectangles indicate regions of anomalous anti-cyclones.

ACPD
12, 1979–2024, 2012

A Tropospheric ozone maximum over the Indian Ocean

L. Zhang et al.

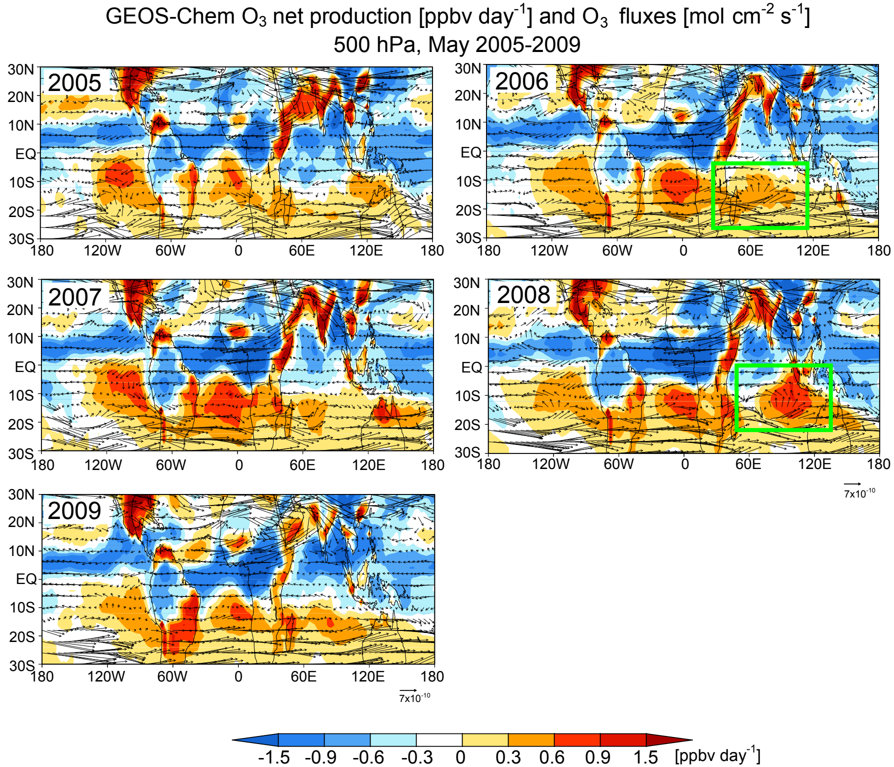

Fig. 17. GEOS-Chem simulated net chemical O_3 production rates (ppbv day^{-1}) and horizontal O_3 fluxes (arrows, mol cm^{-2} s^{-1}) at 500 hPa. Values are monthly means for May 2005 through 2009. Rectangles indicate regions of anomalous anti-cyclones.

ACPD
12, 1979–2024, 2012

A Tropospheric ozone maximum over the Indian Ocean

L. Zhang et al.